FLORE
Repository istituzionale dell'Università degli Studi di Firenze

Cultural heritage microclimate change: Human-centric approach to experimentally investigate intra-urban overheating and numerically

note finali coverpage

(Article begins on next page)

03 February 2025

1 **Cultural heritage microclimate change: human-centric approach to experimentally investigate**

2 **intra-urban overheating and numerically assess foreseen future scenarios impact**

3 Benedetta Pioppi[1], Ilaria Pigliautile[1], Cristina Piselli[1,2], Anna Laura Pisello*[1,2]

4 [1]CIRIAF Interuniversity research centre on pollution and environment Mauro Felli, via G. Duranti

5 63, 06125 Perugia, Italy

6 [2]Department of Engineering, via G. Duranti 93, 06125 Perugia, Italy

7 * Corresponding author: anna.pisello@unipg.it

8 **Abstract**

9 Microclimate change related events affect cities total environment and therefore citizens'

10 wellbeing. In a framework of urban resilience challenge, it is important to guarantee thermally

11 comfortable conditions to dwellers in outdoors but also to preserve cultural heritage masterpieces

12 for tourism and local socio-cultural identity. This work couples an innovative field monitoring at

13 multiple scales and a validated numerical modelling effort to identify indoor and outdoor critical

14 conditions at the present time and in the future, according to IPCC climate change forecast

15 scenarios. The authors focused the attention on the overheating risk of Gubbio historical city center,

16 in central Italy. Experimental data analysis highlights the microclimate granularity of the case study

17 with detected temperature discrepancies up to 2.5°C observed at pedestrian height during the

18 hottest hour, i.e. 2 p.m. Collected data are then used to validate the numerical models of (i) the

19 most significant building of the city and (ii) its surroundings to investigate indoor/outdoor thermal

20 comfort stress due to climate change and local overheating. The combined analysis shows that

21 indoor operative temperature reaches 32°C on average in 80 years, compared to the current 29°C

22 value. In the outdoors, apparent temperature increases by about 10°C on 2100, being responsible

23 for a serious threat compromising socio-cultural life, human health and outdoor and recreational

24 activities.

25

1. Introduction

30   Climate change is considered as one of the most significant hazard of the 21st century [1]. This

31   phenomenon looms as increase in frequency and intensity of extreme weather events [2], such as

32   heat waves, droughts, floods, landslides, cyclones and heavy precipitations in the next future [3].

33   Moreover, anthropogenic actions have been widely acknowledged to be responsible for urban

34   climate alteration, due to land covering modification and greenhouse-gas emissions. The Urban

35   Heat Island (UHI) phenomenon at surface level, i.e. Surface Urban Heat Island (SUHI), which refers

36   to the increase in urban areas surface temperature with respect to the surrounding rural areas, is

37   the evidence of that and it is detected in more than 400 cities worldwide (e.g. Sidney [4], Athens

38   [5], Milan [6], Californian cities [7], Singapore [8] , etc.), and it is responsible for a huge modification

39   of the urban anthroposphere, hydrosphere, biosphere and atmosphere. The analysis of the UHI

40   magnitude show that the UHI intensity can reach 5°C and exceed 8°C [9]. Moreover, synergy

41   between UHI and the increasing frequency, duration and strength of heat waves is demonstrated

42   by Perkins et al [10]. Li and Bou-Zeid show that daytime and nighttime UHI indexes computed during

43   the heat wave period in Baltimore-Washington metropolitan are higher compared to indexes

44   obtained just before the extreme weather event, as demonstrated by means of a combination of

45   observational and modeling analysis [11]. This urban overheating affects the urban livability of the

46   city and it has multiple impacts on energy consumption, environment and pollution, on citizens'

47   health condition and comfort perception, on economy in terms of tourism and human well-being in

48   general [12]. Most of all, urban overheating also involves city centers and dense urban areas,

49   including cultural heritage places, which become increasingly less livable and accessible, with all the

50   consequences on a societal basis. The most documented consequence is the increase of the peak

51   and global electricity demand for heating, ventilation and air conditioning (HVAC) systems.

52   Santamouris et al. examine 30 monitoring profiles of urban and suburban weather stations in

53   Athens, they detect doubled and tripled peak building electricity demand due to UHI [13]. On the

54   other hand, Huang and Gurney quantify the financial implications of climate change to consumers

55   at suppliers and find out energy savings up to 340 $/years in heating dominated climates, while

56   highlight an increase in energy costs up to 231 $/years for warmer states in the U. S. [14].

57   Consequences of urban warming include human health threats and influence on mental well-being

58   and human thermal sensation, i.e. heat and cold stress. Numerous studies show the clear correlation

59   between ambient temperature and mortality, suggesting higher risk of mortality in areas with hot

60   or cold temperature and relatively lower rates in optimal temperature zones [15]. From an

61   economic point of view, tourism, recreation and outdoor activities are strongly influenced and

62   deterred by climate [16], [17], and also their resilience may be impact by the lack of visitability due

63   to local overheating compromising outdoor wellbeing in most of the hot season everywhere. Abed

64   et al. study the role of thermal and physical well-being on potential tourism in Algeria and point out

65   how weather and climate are crucially important factors' in tourism potentiality [17]. Moreover, the

66   perception of climate conditions can change in function of tourists' native country and it has been

67   considered by Salata et al., who combine tourism and climate perceptions by using the MOCI and

68   the PMV indices for local and international tourists, respectively, traveling to three Italian cities, i.e.

69   Venice, Rome and Palermo, in order to manage tourist fluxes [18]. In this panorama, to counteract

70   climate change process and the related multidimensional consequences on economy and wellbeing,

71   the scientific communities put in place a huge effort in developing and implementing several

72   mitigation and adaptation techniques [19]. Among them, the implementation of new materials able

73   to (i) optimize radiative exchanges in terms of solar radiations and environment, i.e. cool roof, cool

74   pavements [20]–[22]or to (ii) store and release solar thermal energy shifted in the time, i.e. phase

75   change materials [23] appear to be very promising or to take advantage from the evapotranspiration

76   contribution [24]–[26], and (iii) the use of greenery, i.e. green roof, presents a high mitigation

77   potential [27]. Moreover, better results are expected and obtained by combining more than a single

78   mitigation strategy, as demonstrated by Mohd Fairuz Shahidan et al. that combine both trees and

79   ground surface materials mitigation technologies and point out a reduction in the average of air

80   temperature by 2.7°C and in the maximum peak by 3.5°C [28]. Despite a huge effort has been done

81   by the scientific community to outline potential climate mitigation strategies, frequently they are

82   not applicable in historical urban context which presents several constraints for its cultural value

83   preservation[30], i.e. any architectural modification is indeed forbidden. Historic urban areas were

84   built for different purposes (e.g. defense issues etc.) and different climatic and demographic

85   conditions, hence their architectural design respects the needs of that era, which often does not

86   meet those of nowadays. For these reasons, the effects of climate change are even more

87   exacerbated in the case of built cultural heritage, since resilience strategies should be investigated

88   in order to preserve urban cultural heritage and even more the livability in city center areas.

89   Moreover, re-use of historic buildings is a common practice nowadays, but the application of active

90   or passive solutions to improve indoor environmental quality is not always feasible due to

91   architectural constrains [31]. Therefore, a continuous monitoring of the indoor conditions is

92   fundamental to ensure comfortable conditions for occupants [32], [33].

93   Moreover, human well-being perception plays an important role in city context driving dwellers

94   habits and tourists flow [34]. For this reason, outdoor thermal comfort interested researchers for

95   decades [35]. Practical indices have been proposed aiming to: (i) consider the wide variety of

96   microclimatic and physiological parameters which influence the perception of each individual and

97   more in general of the community; (ii) grade thermal sensation in outdoors; (ii) evaluate human

98   conditions in various outdoor conditions [36] Nevertheless, this challenge is an ongoing process [36].

99   The pedestrian perspective is still missing; hence it opens scientific investigation possibility.

100 Within the presented framework, this study proposes an innovative methodology coupling

101 multiscale experimental monitoring and numerical modeling strategies to identify critical conditions

102 in terms of heritage site resilience and dwellers/citizens' wellbeing both at inter-building and single-

103 building dimension. The proposed methodology, deeply described in section 2 of the paper, can be

104 summarized as follows:

105 (i)   investigation of the existing, site-specific, microclimate conditions in the heritage site, by

106   means of available weather data and collection of additional information thorough usage of

107   stand-alone and easily-to-install thermohygrometers;

108 (ii)   focus on the pedestrian perspective and assessment of human outdoor and indoor thermal

109   comfort by means of direct and rational comfort indexes calculation;

110 (iii)   extension of the experimentally-driven analysis to future scenarios through numerical

111   modelling and the adoption of forecasted weather forcing taking into account the on-going

112   process of climate change according to IPCC scenarios.

113 The above-mentioned procedure allows to highlight the most critical areas within a specific case

114 study and to point out potential worsening in comfort perception inside public heritage buildings.

115 The final goal is therefore to address local policy-makers towards tailored strategies to enhance the

116 livability of the site and the preservations of its monuments. The authors present such methodology

117 applied to the city center of Gubbio, a Medieval hilly town in Italy, and more specifically to its most

118 touristic building facing the town main square, i.e. Palazzo dei Consoli. According to the Koppen

119 and Geiger classification [37], Gubbio climate is *Cfb* that stands for temperature climate in the

120   middle latitude with absence of a dry season and presence of rainfall every month of the year. In

121   general temperatures belonging to this category in the coldest month are higher than -3°C and

122   below 18°C, in addition, at least a month is characterized by air temperature average of 10°C. A

123   detailed description of the case study is given in section 3. Outputs of both the experimental

124   campaigns and the numerical analysis are presented in section 4 and final conclusions and

125   potentials of the method are pointed out in section 5.

126   Therefore, the novel contribution of the work consists of the integration of a per-se novel

127   environmental monitoring technique that, for the first time, is able to detect the pedestrian

128   perspective on microclimate scenarios in the indoors and outdoors, with classic monitoring

129   campaigns useful for the calibration and validation of numerical models run for climate change

130   prediction scenarios. This technical procedure is then aimed at providing reliable and useful data

131   for policy makers and other stakeholders (public authorities, etc.) who may better understand

132   population fluxes and increase in morbidity related to climate change hazards, responsible for social

133   life modifications in the outdoors. The proposed approach may guarantee a wide replicability

134   potential in dense historical cities, which are often neglected while developing and implementing

135   UHI mitigation techniques and are becoming increasingly less resilient to climate change related

136   events.

137

138   **2. Methodology**

139   This study aims to present a method for the microclimate investigation of heritage sites coupling in

140   field monitoring and numerical modelling at different scales through the following steps:

141   (i)   in-field monitoring by wearable systems, specifically designed to this aim,

142   (ii)   In-field monitoring by local permanent weather stations in key points of the urban

143   contexts

144   (iii)   Building scale and inter-building scale modelling and calibration thanks to data collection

145   in (i) and (ii)

146   (iv)   Elaboration of climate change prediction boundaries for both the modelling categories

147   at (iii) and simulation of future climate change forcing scenarios, according to

148   internationally acknowledged reports.

149   The proposed human-centered evaluation perspective is able to identify indoor and outdoor

150   overheating risk at present and in the next future. The methodology approach is resumed in

151   Figure 1 and the following sub-sections deepen each single step of the work-flow.
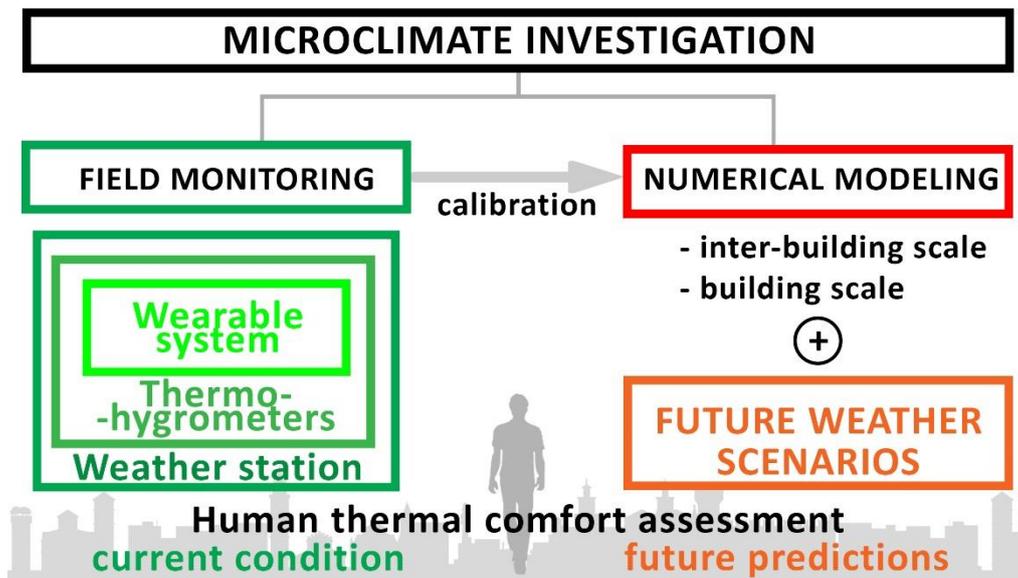
152

153   *Figure 1 Flow-chart of the applied methodology coupling field monitoring and numerical modeling*
154

155   *2.1 Field monitoring*

156   In order to assess the microclimate variability of the case study, the conducted monitoring campaign

157   integrates different monitoring systems, each one focused on a different scale and perspective of

158   analysis. The adopted systems are: (i) a fixed weather station, (ii) stand-alone thermohygrometer

159   probes, and (iii) a new wearable environmental monitoring system[38] .

160
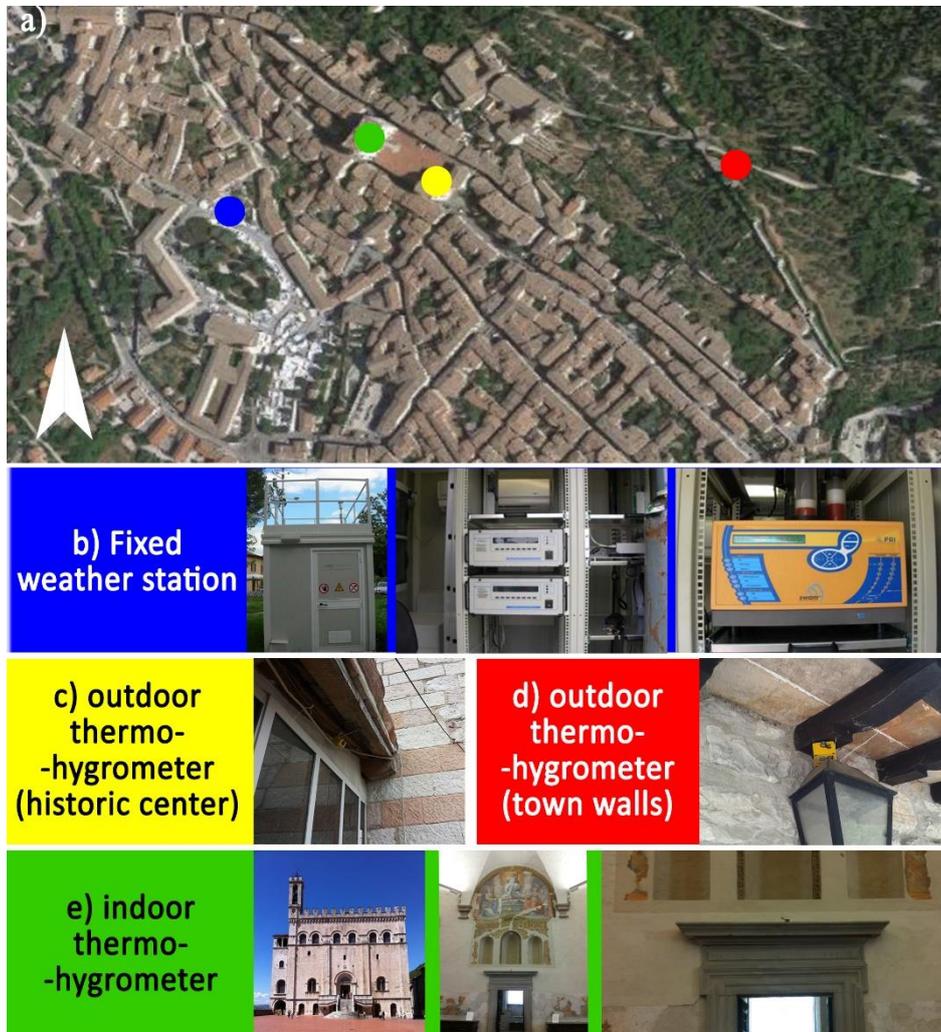
161

162   *Figure 2. a) site-location of the fixed monitoring system involved in the study: (b) fixed weather station, and (c-d-e) three small air*

163   *temperature and humidity stand-alone probes*

164

165   In particular, the fixed weather station is managed by the regional environmental protection agency

166   and is located at the bottom of the town historic center in a green open field area (Figure 2a, b). The

167   station is equipped by a rain gauge, a barometer, a standard wine vane, a pyrometer, an UV-A and

168 UV-B radiometer and provides reading in hourly resolution. These data are mainly used to allocate

169 site-specific and more frequent data collection into a proper weather history of the area.

170 Two thermo-hygrometers are installed close to two selected areas of the case study which are

171 considered as key tourism spots with specific conditions, as shown in Figure 2c, d. In particular, one

172 probe is located within the historic city center, on the terrace of the municipality building facing the

173 main square of the town, while the other probe is located close to the ancient town walls, at the

174 border between the Medieval city and the surrounding woods. An additional temperature probe is

175 located inside the most tourist-attractive heritage building located on the main square of the case

176 study town (Figure 2e). These points are selected also because they were accessible for

177 maintenance, safe and also representative of specific points that will be later used to correlate and

178 validate microclimate models.

179 The adopted probes are small-size, stand-alone dataloggers (Tinytag model TGP-4500). Such

180 instruments are able to monitor values from -25°C to 85°C in temperature and from 0 to 100% in

181 relative humidity. The recording time-step is settled every 10 minutes to guarantee an internal

182 memory capacity of three months. The installation criteria took into account the necessity to shade

183 all the sensors from direct solar radiation, in order to ensure the reliability of the hygrothermal

184 measurements. Therefore, the sensors are ventilated from roofs and facades in order to not be

185 affected by the close proximity to the built environment.

186 Finally, the focus of the environmental monitoring is turned on the pedestrian perspective to deeply

187 examine and detect critical environmental condition in terms of citizens' well-being. To this aim, a

188 detailed monitoring campaign is conducted by means of an innovative wearable monitoring system.

189 This is a miniaturized weather station able to carry out a multiphysics analysis of the urban and

190 suburban areas from the fragile human perspective. It is composed by a series of miniaturized

191 sensors implemented in a specific designed support which has been properly tailored for being

192   installed over a helmet or on a backpack. Its characteristics of light-weight and small-size allow to

193   collect weather data and other microclimate parameters along cities transects and other

194   environment that are not accessible for commonly used transportation vehicles [38]. Moreover,

195   data collected by such human-centered monitoring device are particularly suitable to get a more

196   accurate investigation of human thermal perception in outdoors [38].

197   From a technical point of view, the system collects all the parameters reported in Table 1 every 2

198   seconds. Additionally, it is equipped by an infrared and a visible camera, and a GPS antenna which

199   allows to link all the collected environmental parameters to their specific location in terms of

200   latitude, longitude, altitude, and attitude, i.e. roll, pitch and yaw (Figure 3).

201

Monitored parameter	Technical specifications
Air Temperature [°C]	Absolute accuracy: ±0.5°C at 25°C
	Response time: 1s
Relative Humidity [%]	Absolute tolerance: ±3%
	Response time: 1s
Atmospheric Pressure [hPa]	Sensitivity error: ±0.25%
	Response time: 1s
Global Solar Radiation [W/m^2]	Spectral range: 360÷1120 nm
	Calibration uncertainty: ±5%
Lighting [lux]	Spectral error: 2.3%
	Response time < 1ms
Wind speed [m/s]	Operational range: 0.25 ÷ 40 m/s
	Resolution: 0.1 m/s
	Sensitivity: 0.13 m/s

	Output rate: 2 Hz
Wind direction [deg]	Resolution: 1°
	Sensitivity: ± 1°
	Output rate: 2 Hz
CO_2 concentration [ppm]	Accuracy: ± 2% full scale
	at 20°C and 1000 hPa
	Response time (T_{90}): < 30s
CO concentration [ppm]	Measurement range: 0 ÷ 2000 ppm
	Resolution < 0.5 ppm
	Response time (T_{90}): < 30s
VOC concentration [kOhm]	Response time (T_{90}): ≤ 15s
GPS coordinates	Horizontal spatial accuracy: 2.5m

202

203 *Table 1 Parameters collected by the innovative wearable monitoring system*[38]
204

205 The system has also a Wi-Fi access that allow to connect the monitoring system and visualize over

206 real time the collected environmental parameters and to initialize a record session. The outcomes

207 allow to spatially investigate the microclimate variability of the area and to estimate the human

208 well-being of the pedestrian which is one of the main goals of this work.
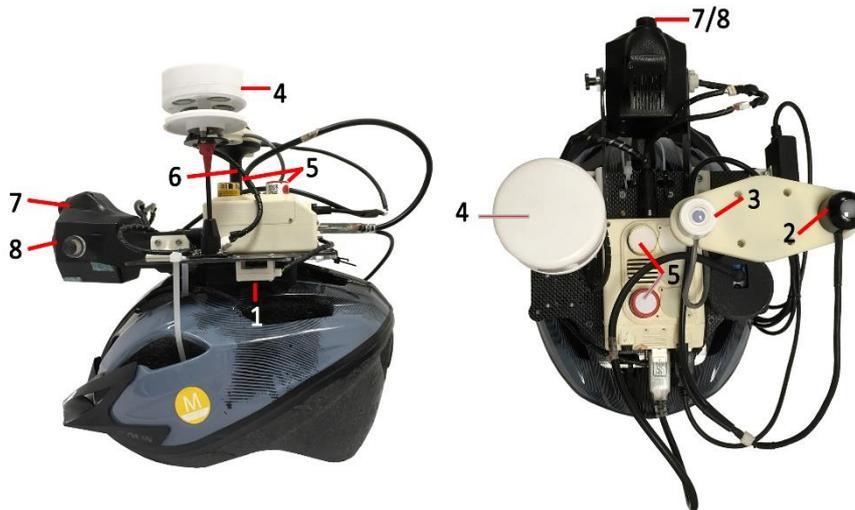
1)Thermo-hygrometer; 2) Pyranometer; 3) Luxmeter; 4) Anemometer;
5) CO_2/CO/VOC concentration; 6) GPS; 7) Visible camera; 8) Infrared camera

Figure 3. Overview of the designed monitoring system settled upon a common bike helmet

The detailed monitoring campaign is performed in a sunny summer day, i.e. August 2nd and the same pathway is repeated for three times, i.e. around sunrise, around midday and around sunset, in order to have the spatial and temporal variation of the key environmental parameters. For security reasons, since the selected pathways include parks and other potentially dangerous areas to cover during the night-time, the very last measurements are performed around sunset, i.e. 6-7 p.m. Therefore, the night-time data are gathered from simulation, permanent station and sensors that showed a negligible impact in terms of air temperature values.

The chosen pathway (Figure 4) is previously planned in order to pass through different urban spaces in terms of (i) urban geometry, (ii) canyons orientation, (iii) anthropogenic sources, and (iv) greenery. The length of the pathway is walkable in less than one hour and therefore it is assumed that the detected variability of the environmental parameters is only spatially-driven, with negligible time dependency.

224

Figure 4 The chosen pathway covered by the wearable system

226

2.2 Numerical modeling

2.2.1. Numerical microclimate modeling and validation

In order to (i) support the main findings of the experimental campaigns in terms of intra-urban

microclimate variability and (ii) extend such findings in time taking into account the main frame of

the climate change, microclimate numerical simulations are performed by means of ENVI-met V4

tool, which is a holistic three-dimensional non-hydrostatic simulation engine able to reproduce the

microclimatic and physical behavior of urban and rural spaces [39]. The mentioned tool is often

used to reproduce and simulate the urban and intraurban environment [40] and it is considered to

be the most suitable for the goal of the current work. The model geometry is realized by

considering the Arakawa C-grid numerical discretization, both the vegetation and the soil are

schematized as one-dimensional column with a certain height and a given respectively leaf and

root normalized area density profile. The interaction between the plant and the surrounding air

can be provided in terms of direct heat flux, evaporation flux and transpiration flux; while the soil

240   types and surfaces can be assigned for each grid cell considering the individual thermodynamic

241   and hydraulic properties.

242   A global analysis can be carried out and it allows to determine air temperature, relative humidity,

243   global radiation, and mean radiant temperature values within the modeled area [39]. The outdoor

244   air temperature and relative humidity are based on the 3-D wind field which is described as three-

245   dimensional turbulent flow given by the non-hydrostatic incompressible Navier-Stokes equations

246   [41]. Moreover, the distribution of temperature and specific humidity of the atmosphere is

247   controlled by the combined advection-diffusion equation with internal source or sinks [41]. The

248   calculation engine is also able to calculate the radiative fluxes, the incoming shortwave and

249   longwave radiation are calculated by two-stream approximations and some empirical formula [42].

250   The concept of reduction coefficient is used to shape the variation of inside radiation linked to

251   absorption by plants or shading by building [41].The interaction between the built surfaces and the

252   atmosphere con be carry out considering all the thermos-physical properties as input parameters,

253   i.e. thickness, albedo, thermal emissivity, absorption capability, transmission capability, heat

254   transfer coefficient and heat capacity.

255   In order to get output referring to human perspective, the authors decide to adopt a spatial

256   resolution of 2 m on the three axes, i.e. 2 m units for both horizontal and vertical grids. Due to the

257   adopted constrains, the final model refers only to a portion of the experimentally monitored

258   environment. In particular, the modeled area is centered on the main square of the Gubbio historic

259   center, where the most touristic building faces, and its close surroundings (Figure 5 a). The area is

260   characterized by strong height variation of the terrain, and therefore the elaboration of a specific

261   digital elevation model was necessary to discretize the ground slope. The adopted materials are

262   specifically created in order to faithfully represent the real thermal properties and condition of the

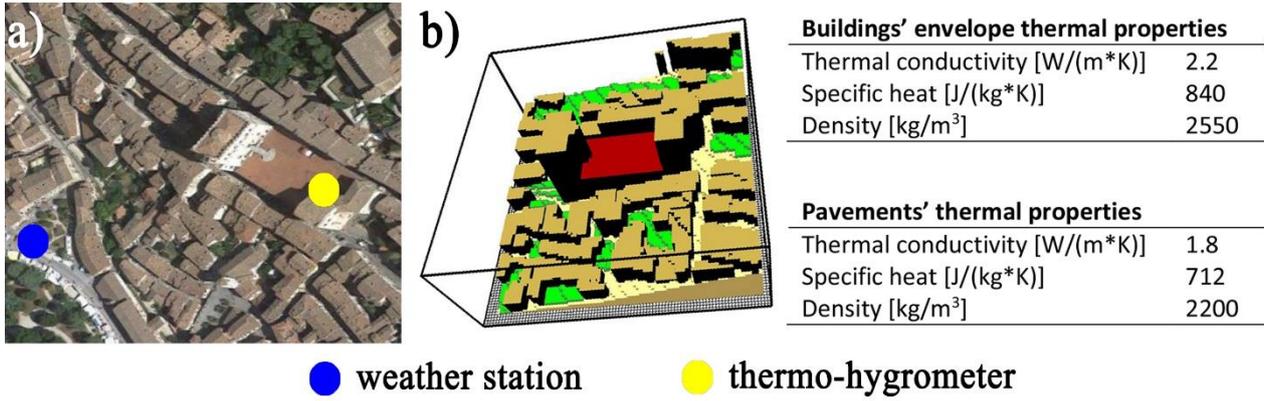263   area as it is summarized in Figure 5.

Buildings' envelope thermal properties	
Thermal conductivity [W/(m*K)]	2.2
Specific heat [J/(kg*K)]	840
Density [kg/m³]	2550

Pavements' thermal properties	
Thermal conductivity [W/(m*K)]	1.8
Specific heat [J/(kg*K)]	712
Density [kg/m³]	2200

🔵 weather station   🟡 thermo-hygrometer

Figure 5 (a) Site locations of references weather data for (b) microclimate model calibration

The data collected by the fixed weather station are used as weather forcing for the simulation in terms of 24 hours air temperature and relative humidity profile and initial wind speed and direction at 10 m height from the ground. The simulation time step is chosen in order to avoid turbulence issues. Hence, the simulation started during the night with weak turbulence condition and the duration of each simulation is 48 hours, in order to provide 24 hours of spin-up (i.e. initialization period for the CFD calculation), reduce any numerical error in the results, and increase the model accuracy [43].

The simulation results are then compared to the observed air temperature data collected by a single thermo-hygrometer in order to validate the models through the calculation of three of the most used calibration indexes [44] which are (i) Mean Bias Error, and (ii) Root Mean Square Error computed accordingly to the following equations:

$$\text{MBE} = \frac{\sum_{j=1}(P_j - O_j)}{N_D} \qquad (1)$$

$$RMSE = \frac{\sum_{j=1}(P_j - O_j)^2}{N_D} \qquad (2)$$

where P_j and O_j are the model-predicted and observed variables for each j-th instant and N_D is the number of analyzed data.

282

2.2.2. Dynamic thermal-energy model of the heritage building

In order to evaluate tourists' indoor thermal perception in heritage buildings, the thermal-energy model of the most attractive historical building of the case study is developed within EnergyPlus simulation environment [45]. The model (Figure 6) takes into account the real geometry and materials thermo-physics properties of the historical building. Therefore, the joint of floors characterized by different heights is realistically modelled, yet avoiding architectural finishes that are not relevant for the purposes of the thermal-energy simulation. In details, the external opaque envelope is characterized by thermal conductivity equal to 2.2 W/m K, density equal to 2550 kg/m^3 and specific heat equal to 840 J/kg K. As for the occupancy, the acknowledged UK NCM (National Calculation Method for Non Domestic Buildings) [46] standard model for Museums and similar buildings is considered by varying the activity in each thermal zone according to the real end-use, e.g. services, reception, display and public areas, circulation areas, etc. The occupancy density is defined according to the real average occupancy of the building. Therefore, the model is calibrated by means of air temperature data collected by a stand-alone probe that was installed in the main hall of the building for one month.
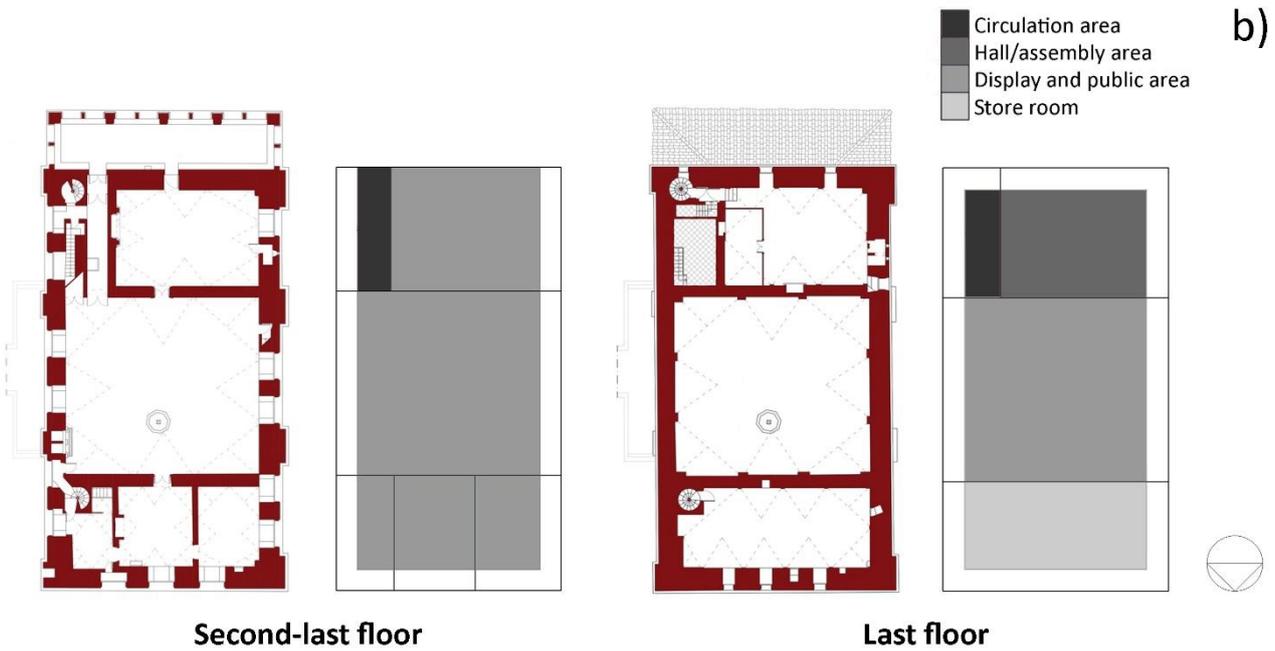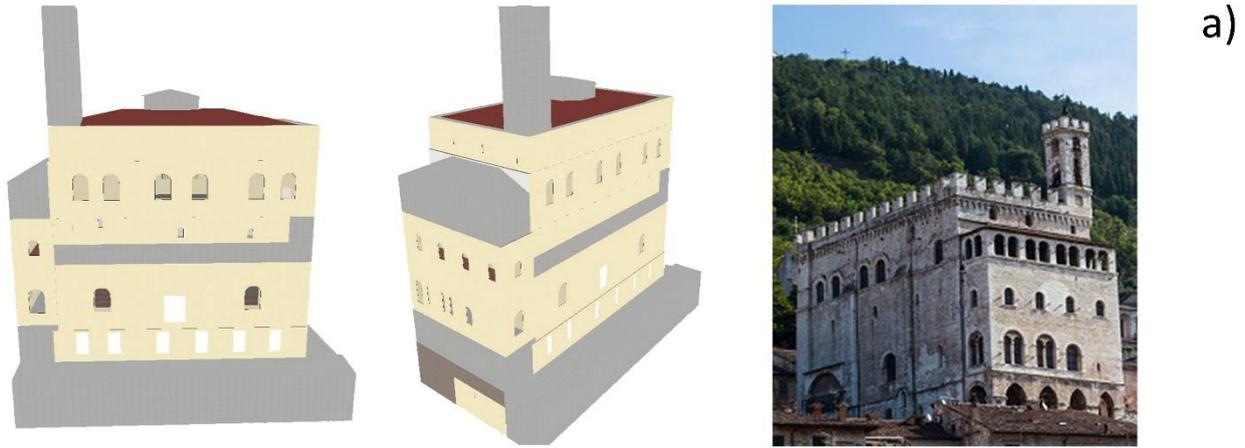
The model validation procedure involves the calculation of the same indexes adopted for the validation of the microclimate model, i.e. MBE and RMSE.

Moreover, the outcomes are analysed in terms of operative temperature, which allow to assess the thermal comfort of the occupants in buildings. This parameter, indeed, describes the combined effects of convective and radiant heat transfer, Accordingly, it can be calculated by means the following equation [47]:

308 $$T_o = \frac{h_r T_{mr} + h_c T_{db}}{h_r + h_c} \qquad\qquad\qquad\qquad\qquad\qquad\qquad (3)$$

309 where h_c and h_r are convective and linear radiative heat transfer coefficient, T_{db} is dry bulb air

310 temperature, and T_{mr} is mean radiant temperature.

311

312 *2.3. Future climate change prediction scenarios*

313 To analyse how climate change from the past to the future can influence the human thermal

314 comfort perception, four weather forcing scenarios are created by means of Meteonorm tool [48]

315 [49], i.e. a database containing global meteorological and climatological data collected by over 8300

316 measuring weather stations with reliable detail of solar radiation, five geostationary satellites and a

317 global calibrated aerosol climatology. This tool is able to generate accurate and representative

318 typical years for any place, since it generates site specific weather data thanks to sophisticated

319 interpolation models based on the data collected by the nearby weather stations and on more than

320 30 years data collections [50].Moreover, the same tool allows to simulate future climate change

321 scenarios according to the International Panel on Climate Change IPCC prediction; in detail in this

322 work three future weather forcing are created according to the scenario A2 described by the IPCC

323 [51], which is the worst one that demonstrates the best reliability prediction in the past 10 years. It

324 forecasts a slow growth of the share capital, slow technological progress, limited social interaction,

325 economic and cultural differences between regions, an uneven economic growth where the gap

326 between industrialized countries and developing countries is wider, increased soil erosion and water

327 pollution, increased global warming and rising sea level [52]. The selected years for the analysis are

328 2020,2050 and 2100. Moreover, a past scenario taking into account as irradiation period 1991-2010

329 and as temperature period 2000-2009, is created in order to have a reference data. Therefore, in

330 order to investigate how climate change influences human well-being, especially during summer

331 which is the most touristic season of the year and the most delicate due to overheating risk, typical

332 summer days are selected for each year in order to run the microclimate simulation and analyse the

333 human thermal comfort perception by PET computed by Rayman model [53], [54] .

334 Firstly, the entire summer period, i.e. from June 21st to September 21st, of the created weather files

335 are analysed in terms of cloud cover and air temperature trend in order to select a typical summer

336 day characterized by clear sky conditions and the mean hottest air temperature. Cloudless sky days

337 are preferably chosen, since the adopted simulation tool may be considered as mostly reliable under

338 stable atmospheric conditions. The extreme values of air temperature and relative humidity for the

339 chosen days are listed in Table 2.

340

Year	Air Temperature [°C]		Relative Humidity [%]	
	Maximum	Minimum	Maximum	Minimum
Past (2000-2009)	34.9	22.0	85.5	47.8
2020	34.6	23.5	84.5	46.2
2050	36.0	23.7	93.6	43.6
2100	38.8	29.8	97.4	52.9

341

342 *Table 2 Extreme values of air temperature and relative humidity for the chosen days*

343

344 These weather files are then used as input forcing to run the microclimate simulation environment

345 and to conduct accurate analysis about the relationship between climate change and human well-

346 being in the outdoors.

347

348 *2.4 Outdoor thermal comfort analysis*

349 In order to evaluate how changes in urban thermal environment can affect human well-being, the

350 Apparent Temperature (AT) as well as the Physiologically Equivalent Temperature (PET) are

351 calculated.

352 The apparent temperature is defined as "*the temperature at the reference humidity level producing*

353 *the same amount of discomfort as that experienced under the current ambient temperature,*

354 *humidity, and solar radiation*" [55]. It is a direct comfort index, i.e. directly driven upon

355 environmental data, and it is therefore computed for both the monitored actual conditions and the

356 simulated future scenarios. Essentially, it is an arrangement of the air temperature based on the

357 humidity level and the wind chilling effect, but it does not include the solar radiation contribute in

358 the formula adopted in the current work since the human body net radiation is not an available data

359 according to the monitoring system configuration. The formula to calculate this index is reported

360 below (4) and it is applicable to hot weather conditions [56], [57] :

361 $$AT = T + 0.33 \cdot vp - 0.7 \cdot v - 4.0 \qquad (4)$$

362 Where, T is the dry bulb temperature, *v* the wind speed and *vp* the water vapor pressure in hPa

363 obtained from monitored temperature (T) and relative humidity (RH) through equation (5):

364 $$vp = \frac{RH}{100} \cdot 6.105 \cdot \exp(17.27 \cdot \frac{T}{237.7+T}) \qquad (5)$$

365 The physiologically equivalent temperature (PET) is a rational index which takes into account all the

366 basic thermoregulatory processes of the human body. More in details, PET is based on the thermo-

367 physiological heat balance model called Munich energy balance model for individuals (MEMI) [58].

368 It is applicable to a wide range of real outdoor conditions and is defined by the energy balance

369 equation of human body (6):

370 $$M + W + R + C + E_D + E_{Re} + E_{Sw} + S = 0 \qquad (6)$$

371 where, M is the metabolic rate (internal energy production), W the physical work output, R the net

372 radiation of the body, C the convective heat flow, E_D the latent heat flow to evaporate water into

373 water vapor diffusing through the skin, E_{Re} the sum of heat flows for heating and humidifying the

374 inspired air, E_{Sw} the heat flow due to evaporation of sweat, and S the storage heat flow for heating

375 or cooling the body mass [58]. Each term of the equation is expressed in Watt and can assume

376 positive or negative value in case of, respectively, power gains or losses for the body. The individual

377 heat flow is influenced by environmental parameters, i.e. air temperature (influencing C and E_{Re}),

378 relative humidity (influencing E_D, E_{Re}, E_{Sw}), wind speed (influencing C and E_{Sw}), mean radiant

379 temperature (influencing R) [58].

380 According to the literature, PET neutral sensation is adapted to different climates [59] and the most

381 suitable range for the presented case study is the one shown in Table 3 referring to costal

382 Mediterranean climate with a neutral zone between 20°C and 25°C, as find out from Cohen et al. in

383 [60].

384

Thermal sensation	PET range value [°C]
Very cold	PET ≤ 4
Cold	4 < PET ≤ 8
Cool	8 < PET ≤13
Slightly cool	13 < PET ≤ 18
Neutral	18 < PET ≤ 23
Slightly warm	23 < PET ≤ 29
Warm	29 < PET ≤ 35
Hot	35 < PET ≤ 41
Very hot	PET > 41

385

386 *Table 3 Thermal sensation and corresponding PET range for costal Mediterranean climate.*

387

388 In the current study, the PET thermal index is computed starting from the output of microclimate

389 simulation data. In particular, PET is calculated by means of the RayMan [61]calculation tool by

390 taking into account air temperature, relative humidity, wind speed, short and long radiation fluxes,

391 and the thermo-physiological data of a standard young man whose characteristics are resumed in

392 Table 4, during the course of the simulated time and within the simulated area.

393

Height	Weight	Age	Cloths insulation	Activity
1.75 m	75 kg	35 years	0.5 clo	Walking, 2.5 met

394

395 *Table 4 Subject characteristics for PET calculation*

396

397 Concerning indoor comfort perception, the estimation of overheating risk for visitors of the most-

398 attractive heritage building of the case study is carried out in terms of frequency of simulated hourly

399 air temperature data above comfortable limits during summer season. Particular attention is

400 dedicated to the overheating risk above 30°C, considered as a key threshold affecting human

401 wellbeing [62], [63].

402

403 **3. Description of the case study**

404 Gubbio is a small ancient town located in central Italy (43° 35' N, 12° 57'E) in the North-Eastern area

405 of Umbria Region in Italy centre, which is mostly mountainous, bounded on the east by Apennine

406 mountains and by the Tiber Valley on the west. The urban configuration is typically Medieval with

407 quite narrow urban canyons, i.e. aspect ratio varying between 1.0 and 0.3, and the materials

408 adopted are mainly local stones and terracotta tiles for roofs, i.e. arenaria and bricks.

409   Palazzo dei Consoli is the most important historic monument of the city, designed by Angelo da

410   Orvieto. It was built at the heart of the city in the early 1300s. It is composed by seven floors and

411   characterized by high thickness of the walls, such as ancient buildings, in limestone material, while

412   the floor is realized by terracotta material. Its key city value is also motivated by the fact that it faces

413   the main square of the city where all the main city events usually take place and most of the tourism

414   flux is concentrated.

415   The façade facing the square is divided into three parts by four buttresses. A central fun-shaped

416   staircase leads to the doorway which is flanked by mullioned windows. The upper floor features six

417   arched windows coupled in pairs and adorned with denticulate frames. The top is finished with

418   arches and Guilfe merlons, while on the left there is the battlement bell-tower [64]. The building

419   further peculiarity is that it stands on the mountain slope, hence its foundations were laid on two

420   different level because of the nature of local topography. The difference in altitude between the

421   two levels of the case study area corresponds to 48 meters, starting from an altitude of 501 meters.

422   In this framework, the study focuses on the area surrounding Palazzo dei Consoli to evaluate

423   outdoor and indoor thermal condition especially for tourists and visitors, even under future climate

424   change expected forcing.

425   The climate of Gubbio is *Cfb* according to the climatic classification proposed by Koppen and Geiger

426   [37] which is based on predetermined values of temperature and precipitation calculated according

427   to yearly averages or individual months. The letter *C* means temperate climate in the middle

428   latitude, with balanced heating and cooling prevalence in winter and summer, respectively. The

429   letter *f* indicates the absence of a dry season and highlights presence of rainfall every month of the

430   year. Finally, letter *b* refers to the temperature of the hottest summer month [37].

431

4. Results

4.1 Microclimate field analysis

In this section, all the experimental data collected by means of different monitoring systems are analyzed and integrated. As specified in section 2.1, data involved in the study are (i) the long-term environmental parameters daily profiles extracted from the fix weather station, (ii) time-series of air temperature and relative humidity collected in different and distinctive areas of the case study by means of fix small-size and stand-alone probes, and (iii) the spatial distribution of the main environmental parameters collected during summer overheating monitoring campaign through the wearable, miniaturized system. The integration of these information allows to progressively deepen the assessment of the climatic conditions of the case study with respect to the pedestrian perspective, and therefore to identify the resilience of the historical site with respect to climate change in both the indoors and outdoors.

In detail, Figure 5Figure 7.a reports the daily air temperature data recorded during summer 2017 by the fix weather station. Air temperature trend shows that the selected day for the wearable monitoring campaign, i.e. August 2nd 2017, is within the hottest week of the season, registered during a heat wave event. Therefore, this chosen day can be considered as representative of urban overheating risk.

449
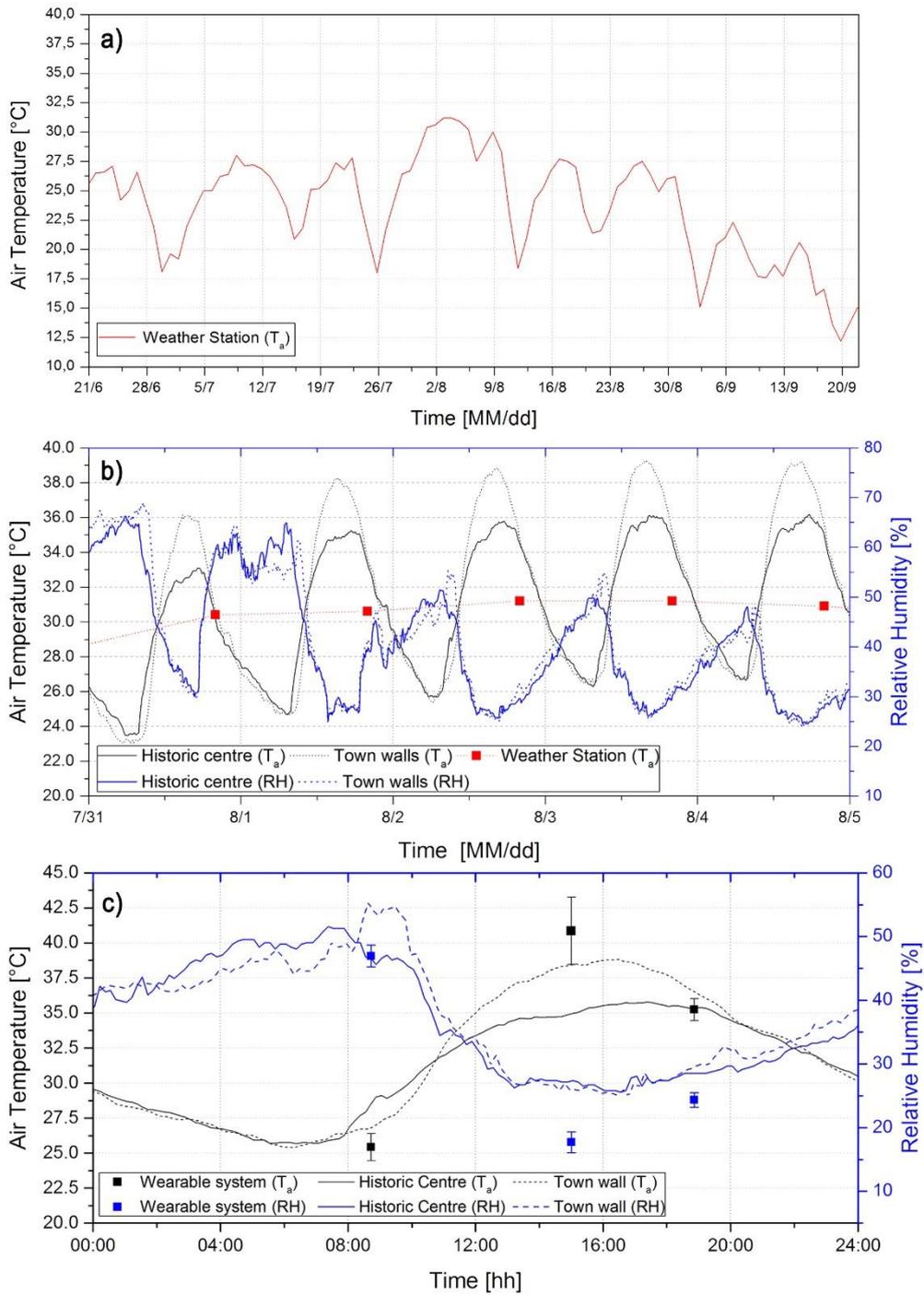
Figure 7.a.b.c d air temperature summer season trend gathered by the fixed weather station located in Piazza Quaranta Martiri (a),

weekly air temperature profiles carried out by the two thermohygrometers and the fixed weather station (b), daily air temperature

profile by the two thermohygrometers overlapped to the mean air temperature values recorded by the wearable system(c)

453

454 Figure 7.b shows air temperature and relative humidity values gathered, from July 31st to August

455 5th, every 10 minutes by the two fix small probes, installed on the terrace of the city municipality

456   building (city center area) and on a private garden house (in the city walls area), respectively. The

457   monitored fluctuations in the two analyzed areas are similar in terms of relative humidity profiles,

458   on the contrary they present a significant deviation in terms of air temperature trends. In particular,

459   air temperature profiles differ up to a maximum of 3.6°C observed at 3 p.m. when data collected in

460   proximity of the town-wall are higher. Moreover, temperature inside the city, i.e. measurement

461   point on the terrace of the municipality building, assumes the highest values at night up to 2.8°C of

462   difference with respect to town-wall temperature reached at 8 a.m.

463   Since the used small probes have the same technical characteristics and they are both shielded from

464   the direct solar radiation and of course they were previously calibrated, these values deviations may

465   be directly imputable to site-specific conditions. Such conditions could be related to the actual wind

466   field and/or solar radiation access to the two sites which contributes to generate peculiar

467   microclimatic conditions even in the same small-scale urban area.

468   The relation between site-specific morphology and microclimate conditions is deepened through

469   the environmental investigation by means of wearable sensing techniques. Figure 7.c presents the

470   outcomes of the wearable monitoring campaign conducted at three different times in the same day,

471   i.e. 8 a.m., 2 p.m., and 6 p.m. on August, overlapped to the small probes recorded trends. In

472   particular, each monitoring session by the payload, is resumed by the mean air temperature value

473   and its standard deviation in terms of error-bar length. This comparison highlights the necessity to

474   perform coupled monitoring, i.e. by means of wearable techniques and classic weather stations,

475   since the special granularity of the collected data may be of interest for better understanding the

476   pedestrian perspective.

477   The average air temperature and relative humidity values at pedestrian level follow the daily time-

478   trend recorded by the fix probes. Nevertheless, the amount of data available from the wearable

479   system depicts a variability of the collected environmental signals which is not appreciable from the

480 small probes data. In particular, standard deviation associated to air temperature data reaches up

481 to a maximum of 2.5°C at 2 p.m. which highlights a significant fluctuation of this parameter along

482 the specifically monitored transect. Such variation highlights the intra-urban microclimate

483 diversification due to morphological differences of the crossed dense urban areas, i.e. different

484 orientation and aspect ratio of canyons, presence or absence of greenery, direct solar availability,

485 etc. In fact, the monitoring perspective in this case switches from the urban canopy layer to, more

486 specifically, the pedestrian height. Such perspective is the most representative to evaluate human

487 thermal wellbeing related data.

488

489   *4.2 Numerical modelling*

490   *4.2.1 Calibration and validation of the microclimate model*

491 The reliability of the realized microclimatic model of the case study area is tested by calculating the

492 MBE and RMSE calibration indexes as previously described. According to data availability and

493 general weather conditions, the selected day to compare the observed field measurement by field

494 monitoring and the simulation results was chosen to be December 1st. The validation procedure

495 takes into account simulated and observed air temperature profiles obtained during December 1st,

496 as shown in Figure 8. Through a calibration procedure, MBR and RMSE indexes obtained are equal

497 to 0.2°C and 0.7°C, respectively. According to the literature and the research effort over the last

498 decade, the obtained indexes outcomes can be considered acceptable [39]. The maximum

499 difference in between measured and simulated air temperature values is 1.5°C. The maximum is

500 registered at peak time as expected since the model does not specifically represent a specific point

501 which is the measured point. Therefore, it can happen that the measured peak time may be higher

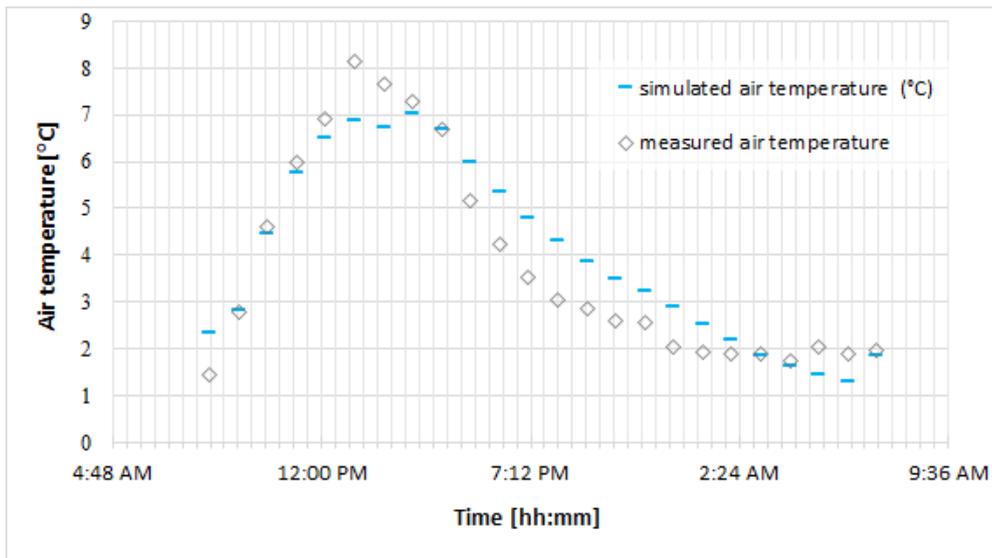502 than the average simulated one within the framework of the cell.

503

Figure 8 Comparison between measured and simulated air temperature trend

504
505

506

507   *4.2.2 Calibration and validation of the heritage building thermal-energy model*

508   Simulated and measured air temperature profiles are compared also for the single building model

509   reliability in predicting the thermal behavior of the heritage building object of the study. The final

510   obtained MBE and RMSE are respectively 0.33°C and 1.07°C. Such results allow to consider the

511   model as acceptable for the scope of this analysis.

512

513   *4.2.3 Microclimate analysis of future scenarios*

514   Maps of Figure 9 (a-c) show air temperature differences between the forecasted future scenarios,

515   i.e. 2020,2050,2100, and the reference one for the modelled area during a typical summer day. The

516   spatial distributions at pedestrian level, i.e. 1.10 meters above the ground, are carried out for three

517   representative moments of the selected day: early in the morning, i.e. at 8.00 a.m., at the time of

518   maximum solar radiation, i.e. 12.00 p.m., and at the time of air temperature maximum peak, i.e. at

519   4.00 p.m. A linear overheating trend, from the past scenario to the furthest future scenario, i.e.

520 2100, is clearly detectable. The highest air temperature difference is expected in summer 2100

521 when an average increase by 3.8°C, 3.6°C, and 3.4°C is obtained at 8 a.m., 12 p.m., and 4 p.m.

522 respectively.

523
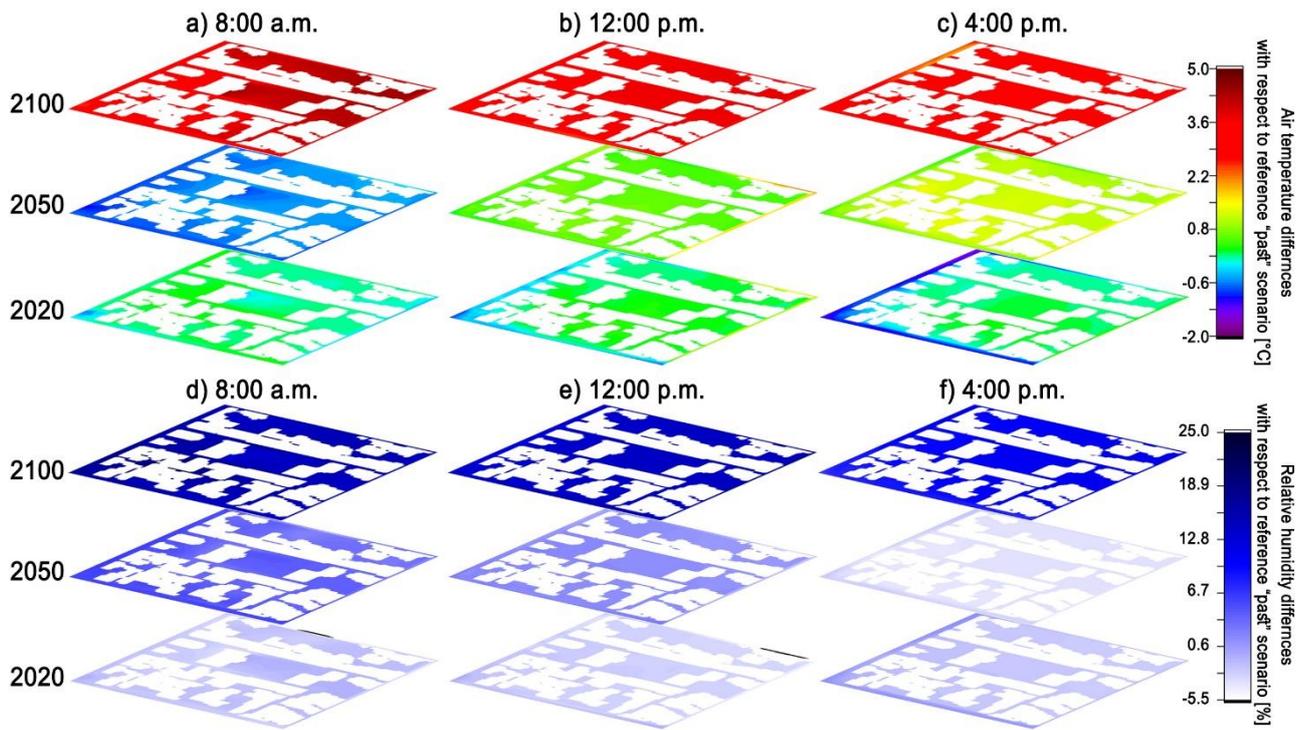
525 *Figure 9 Air temperature (a-c) and relative humidity (d-e) differences between forecasted scenarios, i.e.2020,2050,2100 and the*
526 *reference scenario in summer*

527

528 The same spatial analysis between the foreseen summer future scenarios, i.e. 2020,2050, 2100 and

529 the summer reference one are conducted in terms of relative humidity differences. As illustrated in

530 Figure 9 (d-f), the relative humidity parameter, contrary to the air temperature profile, presents a

531 nonlinear trend from the past reference scenario to the furthest future one, i.e. 2100.

532 More specifically, in summer 2020 as the temperature increases, a decrease in relative humidity is

533 observed. On the contrary, an increase in air temperature corresponds to an increase in relative

534 humidity level in 2100. The maximum relative humidity variation is detected early morning, i.e. 8.00

a.m., in 2100 and it is equal to 15%. This singular behavior highlights the tropical-like increasing

climate trend of the case study area, which makes this analysis even more urgent with the purpose

to identify the cultural heritage resilience to climate change related events.

All the above-observed changes in terms of air temperature and relative humidity between the

reference past and the future scenarios are not related to site-specific morphologies, but allow to

identify the urban scale boundary conditions at the canopy level of the current case study within

the framework of predicted climate change. A spatially averaged value of the outlined differences

can be considered as representative of the forecasted climate change of this area. Therefore, air

temperature and relative humidity spatially-averaged differences between future scenarios and the

reference one are summarized in Table 5.

	ΔT, summer			ΔRH, summer		
	8 a.m.	12 p.m.	4 p.m.	8 a.m.	12 p.m.	4 p.m.
2020	0.1	0.2	0.0	-1.7	-2.5	-1.9
2050	-0.6	0.6	1.1	3.9	1.3	-3.6
2100	3.8	3.6	3.4	15.5	14.0	10.2

Table 5 Spatially-averaged air temperature and relative humidity differences between future scenarios and the reference one at three selected hours, i.e. 8 am., 12 p.m., and 4 p.m.

Cities like the one object of the current study, i.e. almost at the same latitude, are going to

experience hotter and more humid summer according to IPCC. These critical conditions threat

citizens and tourists well-being in outdoors and therefore a detailed analysis of the human thermal

comfort perception is presented in the following session.

555

4.3 Tourist comfort analysis

557 This section is focused on the results of experiments and simulations conducted both in indoors and

558 outdoors, from a pedestrian point of view. The outcomes can be applied to any person living

559 outdoor or indoor, i.e. citizens or tourists. Even though, since Gubbio is a very touristic area and

560 tourists can affect the whole city economy and its resilience to climate change, the current study

561 focused the attention on the tourist perspective.

562

4.3.1 Comfort mapping by means wearable system

564 This section is focused on the experimental wearable campaign results. In detail, the apparent

565 temperature is calculated in order to assume the human thermal perception during a hot summer

566 day in Gubbio historical urban environment.

567 The obtained results are spatially plotted (color scale) with respect to the global solar radiation

568 values by means plot size, as shown in Figure 10.

569
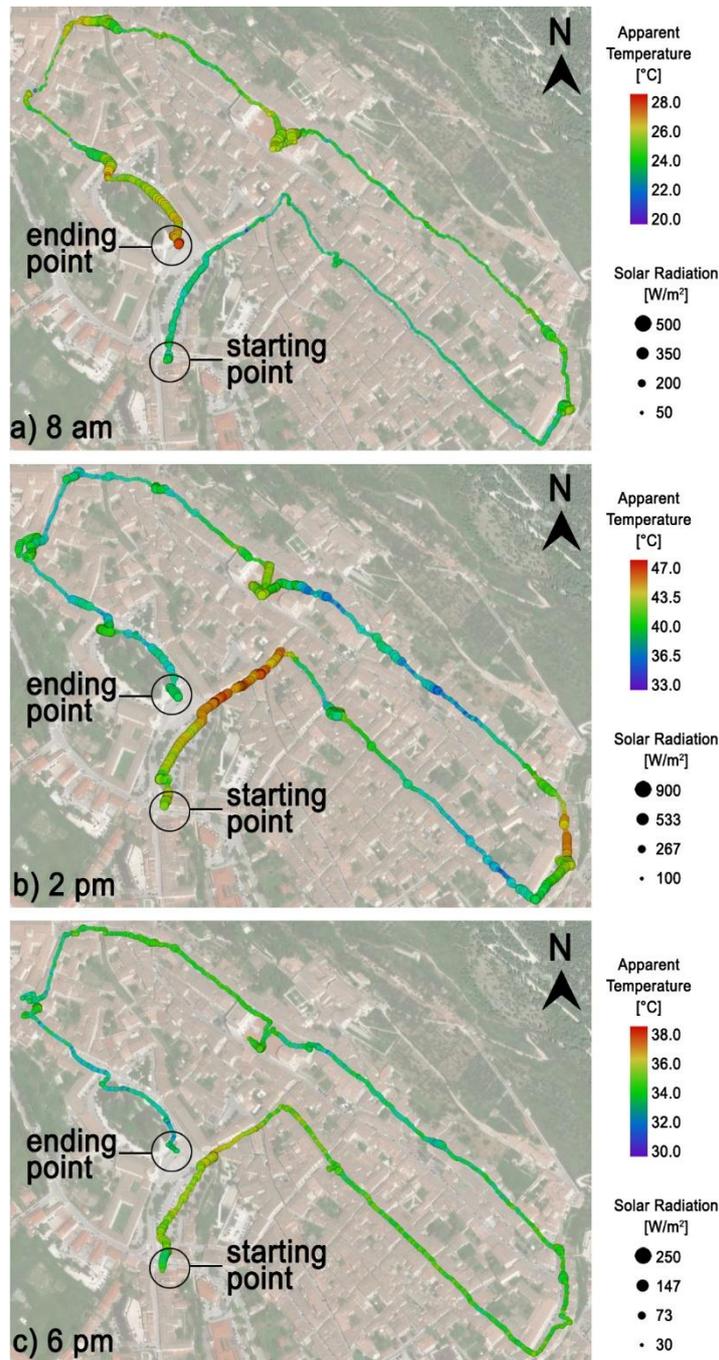
Figure 10 Apparent temperature and global solar radiation maps obtained by means experimental wearable campaign at 8 a.m. (a),

2 p.m. (b), 6 p.m. (c)

As can be seen (Figure 10.a), at 8 a.m. the apparent temperature ranges between 20.10° C and

26.75°C. The maximum values are recorded at the end of the monitoring session when the global

solar radiation is supposed to naturally increase, while the minimum ones are registered at the

beginning 3of the survey campaign, which lead to consider a sort of further time dependence.

However, the spatial distribution of the apparent temperature values is strictly influenced by the urban morphology patterns. In fact, the highest values are gained around squares on the route where sky view factor and incoming global solar radiation assume higher values. Nevertheless, apparent temperature outcomes show acceptable thermal comfort condition which not lead dwellers or tourists to any health hazard all along the monitoring pathway at this moment of the day.

On the contrary, at 2.00 pm the apparent temperature rises up to 46.7°C. As shown in Figure 10.b, the most critical areas (which presents the highest apparent temperature values) are the North-East and South-West oriented canyons, mainly facing the slope toward the southern valley. This orientation allows the direct incoming radiation to access the canyon up to the pedestrian level while high aspect ratios of the same streets limit the energy exchanges towards the sky of both reflected shortwave and re-emitted longwave radiation. This trapping effect leads to an increase of the air temperature. Moreover, the wind chill effect is reduced within packed urban areas. Combination of both the altered radiative budget and the reduction of the convective contribution is responsible for higher human thermal stress perception, i.e. higher apparent temperature values as shown in the plots.

Finally, at 6 p.m., a general decrease of the global solar radiation is detected. Less intense incoming solar radiation leads to smoother fluctuations of air temperature along the monitoring pathway and the monitored built environment looks more homogeneous in terms of air temperature. This thesis is confirmed by the experienced range of apparent temperature, which is equal to 8°c as well as the apparent temperature variation detected at 8 a.m. However, the detected minimum values corresponded to 30°C, versus 20°C, i.e. minimum value at 8 a.m. This is imputable to the urban fabrics configurations and materials that are overheated during the day and tends to slowly release all the stored heat, due to their thermal capacity.

602

4.3.2 Outdoor Thermal comfort perception: actual conditions and future forecast

Thanks to data availability, Figure 11 shows the spatial distribution of the calculated apparent and

physiological equivalent temperature during the hottest summer day as it is foreseen by the IPCC

forcing scenarios.
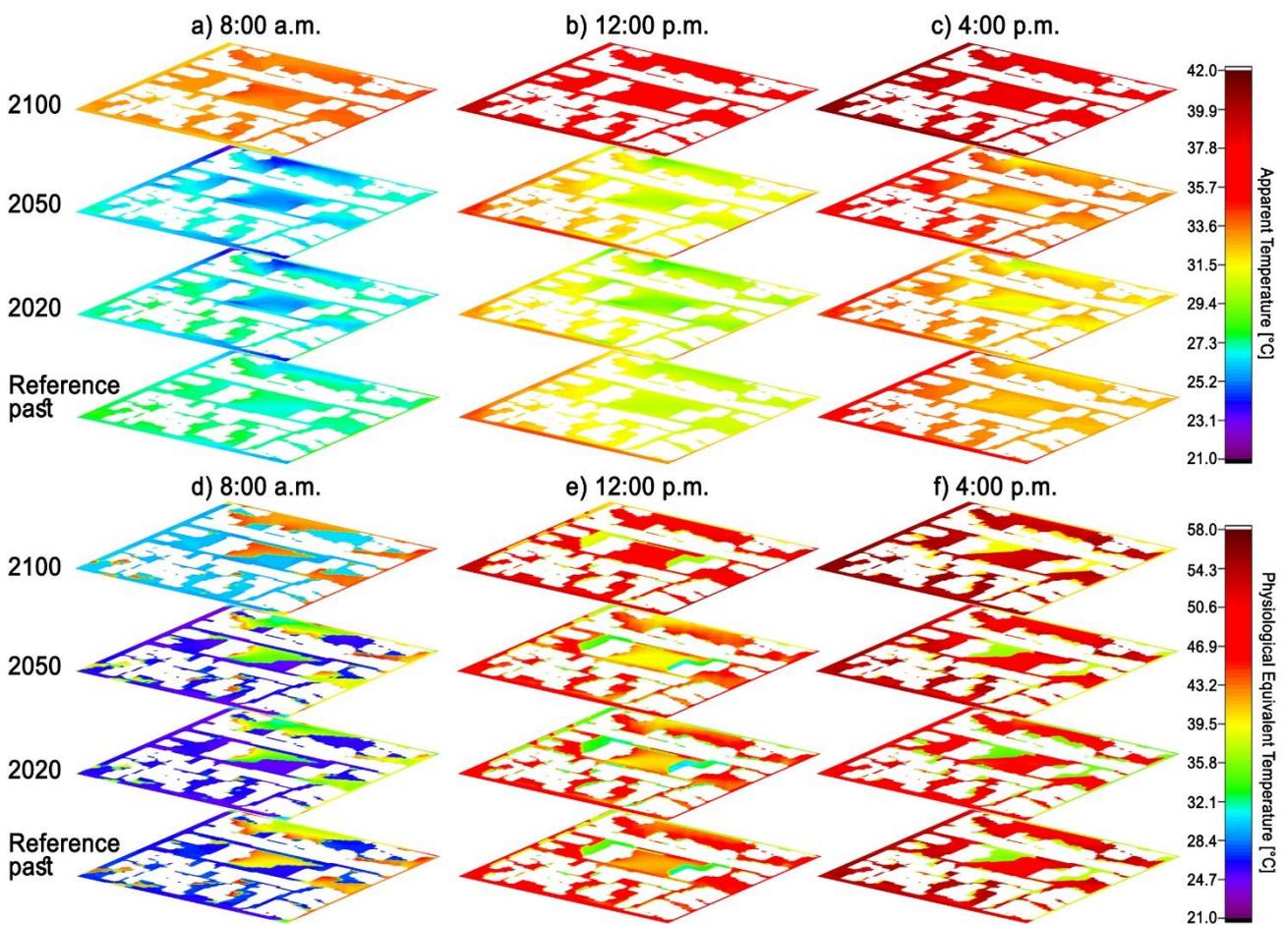
Figure 11 Spatial distribution of apparent temperature (a-c) and physiological equivalent temperature (d-e) for all the simulated

summer days, i.e. reference past, 2020, 2050, and 2100, at 8 a.m. (a,d), 12 p.m. (b,e), and 4 p.m. (c,f).

12.00 p.m. and 4.00 p.m. result are the most critical moments in terms apparent temperature index

and consequentially for outdoors and recreational activities. In detail, a linear increasing in human

thermal discomfort is depicted from the reference scenario to the future scenarios. 2100 is expected

614 to be the most hazardous year due to overheating risk. In fact, the maximum value of AT is predicted

615 in 2100 and it is equal to 42°C, which means very hot sensation and huge level of psychological

616 stress. Spatially, the outcomes show a non-uniform distribution, in particular at 12.00 p.m. on 2020

617 and 2050 low values of AT are expected in the main square area. This fact can be imputable to the

618 wind speed contribution which decreases the air temperature values perception. Moreover, the

619 apparent temperature index is calculated by neglecting the direct global radiation contribution that

620 strictly influences human well-being in open field areas.

621 To fill this gap, the PET index is also calculated to have a more realistic thermal sensation forecast.

622 As can be seen in Figure 11, even PET outcomes show that 12:00 p.m. and 4:00 p.m. are the most

623 risky time of the day. 2100 is revealed to be the worst forecasted year in terms of human thermal

624 perception. From a spatial point of view, directly irradiated areas of the main square are revealed

625 to be exposed to the greatest risk of overheating.

626

627 *4.4 Indoor thermal comfort perception: actual conditions and future forecast*

628 Crossing the building heritage envelope, here the focus is to understand climate change related

629 impact in the indoors of the key building of the historical city under investigation. To this aim, as

630 mentioned, the dynamic simulation model has been run under the same depicted scenarios, i.e. the

631 past, the reference, the 2020, the 2050 and the 2100. Figure 12 shows the operative temperature

632 hourly frequency outcomes obtained at these boundary timings in summer. In particular, the

633 simulated period extends from June 21st to September 21st and it is the most vulnerable period for

634 human thermal discomfort perception, both in indoors and outdoors.

635 As can be seen In Figure 12, in the current scenario the operative temperature exceeds 25°C which

636 is the maximum value allowed to have a thermal comfortable perception in offices environments,

637 according to the EN 15251 [47]. The histogram shows that 28°C and 29°C valued indeed present the

638 highest frequency in the current scenario. In the future, the operative temperature frequency is

639 forecast to increase up to 29°C. On 2050 the operative temperature value of 29°C is expected to be

640 repeated for more than 500 hours during the summer period during the course of the day, while in

641 2080 the most frequent operative temperature is foreseen to be equal to 30°C, reaching the

642 dangerous threshold temperature for most of the time. 2100 is predicted to be even worse, because

643 the average frequency of operative temperature expected will be 32°C and further peaks at 36°C

644 will be expected, which means great level of human thermal discomfort and, in general, lack of

645 livability in the indoors without HVAC systems operating, and high level of psychological stress for

646 tourists and dwellers in general.

647
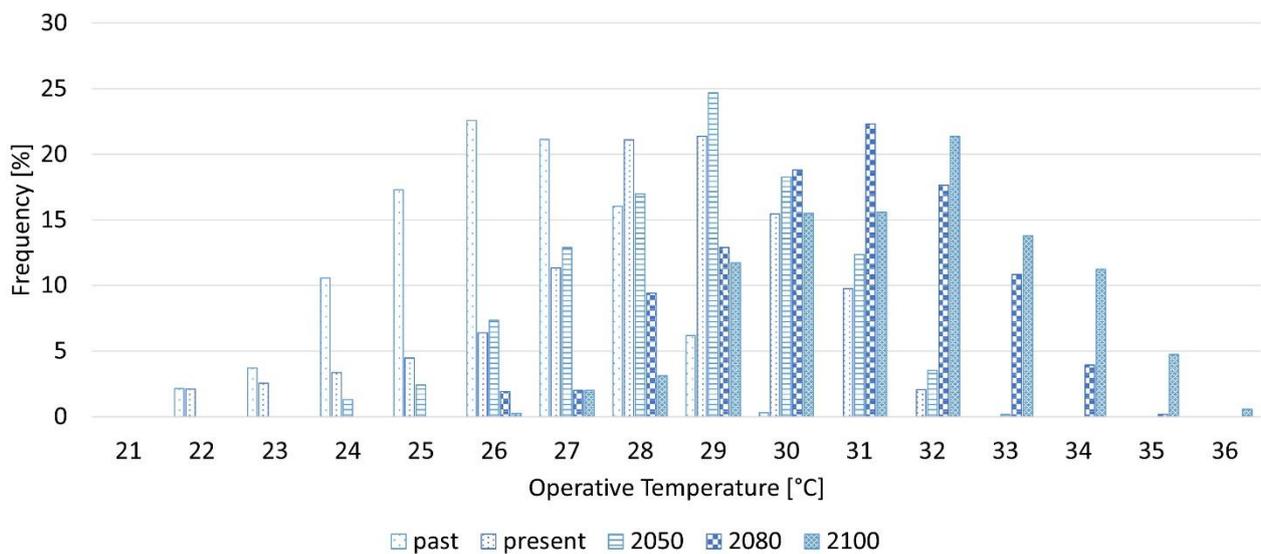
648

649 *Figure 12.* Frequency distribution of obtained hourly operative temperature during summer for all the foreseen scenario simulated.

650

651 **1. Discussion**

652 The focus of the presented research consists of identifying the human perspective in the urban

653 environment affected by anthropogenic actions, responsible for local climate change and air quality

654 damaging. In this view, wearable sensing techniques and microclimate modelling provided a reliable

655 and novel coupled techniques aimed at defining the current and future situation, and its

656 responsibility on building energy need, cultural heritage conservation and, in general,

657 environmental analysis at citizens' level, for better resilient cities and outdoors. In fact, climate

658 change demonstrated to produce an undeniable impact on the total environment, cities and society

659 in terms of human wellbeing and, in most of ancient European cities, it is responsible for heavy

660 tourism drawbacks due to overheating, also impacting the economic sustainability of cultural

661 heritage sites and, more in general, their resilience. Cultural sites are heavily affected by climate

662 change related events, i.e. Urban Heat Island and overheating risk, since the great number of

663 mitigation strategies studied and exploited in the field are often inapplicable in historical city centers

664 due to cultural value preservation constraints. In this context, climate change evaluation and its

665 future progress prediction are crucial to identify outdoor and indoor thermal critical conditions for

666 humans, and to manage tourist flows in thermally comfortable areas of the city improving the urban

667 visitability and guaranteeing their resilience. Therefore, this manuscript proposes an innovative

668 methodology, specifically implemented in the field, with the purpose to investigate historical urban

669 outdoor and indoor conditions coupling extensive and multidimensional experimental monitoring

670 with calibrated numerical modeling of the indoor and outdoor dynamics. In more detail, the climate

671 survey monitoring campaign conducted by fixed weather station, small probes and an innovative

672 wearable system highlights how the climate monitoring scale influences the microclimate analysis

673 and the capability to detect microclimatic variability within the urban context, mostly responsible

674 for outdoor societal life and economic activities. More specifically, fixed weather station data allow

675 to have an annual and seasonal trend of the main environmental parameters, such as air

temperature and relative humidity, but are not able to catch the microclimate variability that

characterize complex heterogeneous urban environment. To this aim the climate survey scale can

be reduced and therefore two stand-alone small probes are located in neighboring areas

highlighting key differences between the two selected areas in terms of air temperature and relative

humidity values. However, a detailed monitoring campaign by wearable system is fundamental to

have the pedestrian perspective and assess the human outdoor thermal comfort throughout the

city, at the required small granularity affecting outdoor societal activities in the hotter seasons. On

the other hand, future climate change scenarios are then necessary in order to predict the evolution

of such microclimate and mesoclimate conditions in the near future. That is the reason why, each

indoor and outdoor validated model may be run also with varying boundary conditions, according

to any future prediction of climate change. For the purpose of this paper, the A2 scenario elaborated

by the IPCC has been selected as the most reliable one in the last years. Therefore, overheating risk

may be assessed in both the indoors and outdoors, preparing the ground for any multidisciplinary

assessment such as the economic investigation of climate change related issues produced on local

tourism activity and so on. The same may be investigated in the indoors where museum spaces or

new operations take place, which can be compromised by climate change progress even in the near

future. In fact, it is very much clear that starting from the next decades, the most probable indoor

operative temperature is higher than 29°C, exacerbating indoor overheating risks for employees and

tourists. In this view, the granular field monitoring data, coupled to microclimate modelling and

prediction of climate change, represented a novel, multiscale and integrated method for

investigating cultural heritage resilience to climate change, in terms of conservation boundaries,

visitability and wellbeing of tourists, representing a key motivation to keep cultural heritage areas

more livable and economically sustainable. Data granularity allowed indeed to frame real

pedestrians' boundary conditions affecting personal feelings and behaviors, and climate change

700 prediction allowed to frame this anthropogenic forcing toward a future perspective, which should

701 be considered when designing cultural heritage conservation and urban planning actions. Compared

702 to only simulation based works, or building-oriented works, the key add on produced through this

703 research consisted on the human-centric approach in defining indoor-outdoor wellbeing from

704 people perspective, where people (e.g. citizens and tourists) represent the key resilience and

705 economic resource for preserving cultural heritage sites and keeping their livability along the time.

706

707 **2. Conclusion**

708 The proposed multidimensional and multifunctional procedure has been applied on the Medieval

709 City of Gubbio, in central Italy. The field monitoring, conducted at different scales, highlights

710 progressively microclimate peculiarities of the monitored environment. In particular, different air

711 temperature profiles are collected by the two measurement points within the same historic center.

712 These results are explained considering different wind fields and different solar radiation access

713 within the two zones. The pedestrian perspective is deepened during a heat wave event in summer,

714 by means of a wearable environmental monitoring station. Moreover, future weather forecast

715 scenarios are simulated and the obtained output shows that in summer, from the past scenario to

716 the future scenario on 2100, a linear overheating in terms of air temperature and a non-linear trend

717 in terms of relative humidity. Moreover, the model of Palazzo dei Consoli is run under the same

718 scenarios and the results are reported in term of hourly operative temperature frequency for each

719 summer period. The outcomes show that in the future, the value of the most frequent indoor

720 operative temperature will increase from 29°C (today) up to 32°C on 2100, with peaks at 36°C in

721 2100, which means high level of thermal discomfort. Moreover, to investigate the human thermal

722 perception, two thermal indexes are calculated by taking into account the environmental

723 parameters collected by the wearable system and the weather condition foreseen according to the

724   IPCC prevision. South-facing spaces and highest sky-view-factor areas are shown to be the most

725   critical areas for citizens or tourists visiting the city in the central hours of the day. Outdoor comfort

726   indexes (apparent temperature) are computed for the predicted future scenarios coupled to the

727   calculation of the rational comfort index physiological equivalent temperature, i.e. PET. The

728   apparent temperature outcomes demonstrate that 12.00 p.m. and 4.00 p.m. are the most critical

729   moments of the day, i.e. 42°C, and a linear increasing in human thermal discomfort is depicted from

730   the past to the future 2100, which is expected to be the most hazardous time. The PET results

731   confirmed this trend and they highlighted the spatial variability of the values, with peaks higher than

732   50°C, highlighted that the main square of the city – the key tourism and citizenship attraction

733   position – is exposed to the greatest risk of overheating.

734   Concluding, the proposed analysis procedure and application to a field study demonstrated to

735   prepare a useful ground to understand the human perception both in indoors and outdoors within

736   cultural heritage places affected by climate change. Moreover, these considerations could help

737   different categories of end users, such as ministries, local governmental bodies, municipalities,

738   environmental protection agencies, etc. Intra-urban microclimate analysis by means of wearable

739   sensing techniques and numerical modelling may be of key help to better manage and preserve

740   tourism flows and local citizens' wellbeing, e.g. their societal attitudes and community belonging

741   feeling, towards more comfortable outdoor and indoor areas, in order to reduce the human health

742   hazard and to preserve local customs and traditions.

743

752

753   **REFERENCES**

754   [1]   D. Mitchell, C. Heaviside, S. Vardoulakis, C. Huntingford, G. Masato, B. P Guillod, P.

755   Frumhoff, A. Bowery, D. Wallom, and M. Allen, "Attributing human mortality during

756   extreme heat waves to anthropogenic climate change," *Environ. Res. Lett.*, vol. 11, no. 7,

757   2016.

758   [2]   L. Nicholls and Y. Strengers, "Heatwaves, cooling and young children at home: Integrating

759   energy and health objectives," *Energy Res. Soc. Sci.*, vol. 39, no. September 2017, pp. 1–9,

760   2018.

761   [3]   G. A. Meehl and C. Tebaldi, "More intense, more frequent, and longer lasting heat waves in

762   the 21st century," *Science (80-.).*, vol. 305, no. 5686, pp. 994–997, 2004.

763   [4]   M. Santamouris, L. Ding, F. Fiorito, P. Oldfield, P. Osmond, R. Paolini, D. Prasad, and A.

764   Synnefa, "Passive and active cooling for the outdoor built environment – Analysis and

765   assessment of the cooling potential of mitigation technologies using performance data from

766   220 large scale projects," *Sol. Energy*, vol. 154, pp. 14–33, 2017.

767   [5]   I. Agathangelidis, C. Cartalis, M. Santamouris, I. Agathangelidis, C. Cartalis, and M.

768   Santamouris, "Integrating Urban Form, Function, and Energy Fluxes in a Heat Exposure

769   Indicator in View of Intra-Urban Heat Island Assessment and Climate Change Adaptation,"

770   *Climate*, vol. 7, no. 6, p. 75, May 2019.

771 [6] R. Paolini, F. Antretter, F. Cotana, A. L. Pisello, M. MeshkinKiya, A. Zani, T. Poli, and V. L.

772   Castaldo, "The hygrothermal performance of residential buildings at urban and rural sites:

773   Sensible and latent energy loads and indoor environmental conditions," *Energy Build.*, vol.

774   152, pp. 792–803, 2016.

775 [7] H. Gilbert, B. H. Mandel, and R. Levinson, "Keeping California cool: Recent cool community

776   developments," *Energy Build.*, vol. 114, pp. 20–26, Feb. 2016.

777 [8] M. Masoudi and P. Y. Tan, "Multi-year comparison of the effects of spatial pattern of urban

778   green spaces on urban land surface temperature," *Landsc. Urban Plan.*, vol. 184, pp. 44–58,

779   Apr. 2019.

780 [9] M. Santamouris, "On the energy impact of urban heat island and global warming on

781   buildings," *Energy Build.*, vol. 82, pp. 100–113, 2014.

782 [10] S. E. Perkins, L. V Alexander, and J. R. Nairn, "Increasing frequency, intensity and duration of

783   observed global heatwaves and warm spells," *Geophys. Res. Lett.*, vol. 39, no. 20, 2012.

784 [11] D. Li and E. Bou-Zeid, "Synergistic interactions between urban heat islands and heat waves:

785   The impact in cities is larger than the sum of its parts," *J. Appl. Meteorol. Climatol.*, vol. 52,

786   no. 9, pp. 2051–2064, 2013.

787 [12] I. Livada, A. Synnefa, S. Haddad, R. Paolini, S. Garshasbi, G. Ulpiani, F. Fiorito, K.

788   Vassilakopoulou, P. Osmond, and M. Santamouris, "Time series analysis of ambient air-

789   temperature during the period 1970–2016 over Sydney, Australia," *Sci. Total Environ.*, vol.

790   648, pp. 1627–1638, 2019.

791   [13]   M. Santamouris, N. Papanikolaou, I. Livada, I. Koronakis, C. Georgakis, A. Argiriou, and D. N.

792   Assimakopoulos, "On the impact of urban climate on the energy consuption of building,"

793   *Sol. Energy*, vol. 70, no. 3, pp. 201–216, 2001.

794   [14]   J. Huang and K. R. Gurney, "Impact of climate change on U.S. building energy demand:

795   Financial implications for consumers and energy suppliers," *Energy Build.*, vol. 139, pp. 747–

796   754, 2017.

797   [15]   A. J. McMichael, R. E. Woodruff, and S. Hales, "Climate change and human health: Present

798   and future risks," *Lancet*, vol. 367, no. 9513, pp. 859–869, 2006.

799   [16]   J. Rodríguez-Algeciras, A. Tablada, and A. Matzarakis, "Effect of asymmetrical street canyons

800   on pedestrian thermal comfort in warm-humid climate of Cuba," *Theor. Appl. Climatol.*, vol.

801   133, no. 3–4, pp. 663–679, 2018.

802   [17]   S. S. Abed and A. Matzarakis, "Quantification of the Tourism Climate of Algeria based on the

803   climate-tourism-information-scheme," *Atmosphere (Basel).*, vol. 9, no. 7, 2018.

804   [18]   F. Salata, I. Golasi, R. Proietti, and A. de Lieto Vollaro, "Implications of climate and outdoor

805   thermal comfort on tourism: the case of Italy," *Int. J. Biometeorol.*, 2017.

806   [19]   R. Freeman and M. Yearworth, "Climate change and cities: problem structuring methods

807   and critical perspectives on low-carbon districts," *Energy Res. Soc. Sci.*, vol. 25, pp. 48–64,

808   2017.

809   [20]   M. Santamouris, "Using cool pavements as a mitigation strategy to fight urban heat island -

810   A review of the actual developments," *Renew. Sustain. Energy Rev.*, vol. 26, pp. 224–240,

811   2013.

812   [21]   F. Rossi, F. Cotana, M. Filipponi, A. Nicolini, S. Menon, and A. Rosenfeld, "Cool roofs as a

813   strategy to tackle global warming: economical and technical opportunities," *Adv. Build.*

814   *Energy Res.*, vol. 7, no. 2, pp. 254–268, 2013.

815   [22]   A. H. Rosenfeld, H. Akbari, J. J. Romm, and M. Pomerantz, "Cool communities: Strategies for

816   heat island mitigation and smog reduction," *Energy Build.*, vol. 28, no. 1, pp. 51–62, 1998.

817   [23]   A. L. Pisello, E. Fortunati, C. Fabiani, S. Mattioli, F. Dominici, L. Torre, L. F. Cabeza, and F.

818   Cotana, "PCM for improving polyurethane-based cool roof membranes durability," *Sol.*

819   *Energy Mater. Sol. Cells*, vol. 160, pp. 34–42, 2017.

820   [24]   A. de Gracia, L. Navarro, J. Coma, S. Serrano, J. Romaní, G. Pérez, and L. F. Cabeza,

821   "Experimental set-up for testing active and passive systems for energy savings in buildings –

822   Lessons learnt," *Renew. Sustain. Energy Rev.*, vol. 82, pp. 1014–1026, 2018.

823   [25]   J. Coma, G. Pérez, A. de Gracia, S. Burés, M. Urrestarazu, and L. F. Cabeza, "Vertical

824   greenery systems for energy savings in buildings: A comparative study between green walls

825   and green facades," *Build. Environ.*, vol. 111, pp. 228–237, 2017.

826   [26]   G. Pérez, J. Coma, S. Sol, and L. F. Cabeza, "Green facade for energy savings in buildings: The

827   influence of leaf area index and facade orientation on the shadow effect," *Appl. Energy*, vol.

828   187, pp. 424–437, 2017.

829   [27]   M. Santamouris, "Cooling the cities - A review of reflective and green roof mitigation

830   technologies to fight heat island and improve comfort in urban environments," *Sol. Energy*,

831   vol. 103, pp. 682–703, 2014.

832   [28]   M. F. Shahidan, P. J. Jones, J. Gwilliam, and E. Salleh, "An evaluation of outdoor and building

833   environment cooling achieved through combination modification of trees with ground

834   materials," *Build. Environ.*, vol. 58, pp. 245–257, 2012.

835   [29]   J. Xu, Q. Wei, X. Huang, X. Zhu, and G. Li, "Evaluation of human thermal comfort near urban

836   waterbody during summer," *Build. Environ.*, vol. 45, no. 4, pp. 1072–1080, 2010.

837   [30]   V. L. Castaldo, F. Rosso, I. Golasi, C. Piselli, F. Salata, A. L. Pisello, M. Ferrero, F. Cotana, and

838   A. De Lieto Vollaro, "Thermal comfort in the historical urban canyon: The effect of

839   innovative materials," in *Energy Procedia*, 2017, vol. 134, pp. 151–160.

840   [31]   G. Leijonhufvud and A. Henning, "Rethinking indoor climate control in historic buildings: The

841   importance of negotiated priorities and discursive hegemony at a Swedish museum,"

842   *Energy Res. Soc. Sci.*, vol. 4, no. C, pp. 117–123, 2014.

843   [32]   A. L. Pisello, A. Petrozzi, V. L. Castaldo, and F. Cotana, "On an innovative integrated

844   technique for energy refurbishment of historical buildings: Thermal-energy, economic and

845   environmental analysis of a case study," *Appl. Energy*, vol. 162, pp. 1313–1322, 2014.

846   [33]   R. Oliveira, J. Lopes, H. Sousa, and M. Abreu, "A system for the management of old building

847   retrofit projects in historical centres: the case of Portugal," *Int. J. Strateg. Prop. Manag.*, vol.

848   21, no. 2, pp. 199–211, Apr. 2017.

849   [34]   L. Chen and E. Ng, "Outdoor thermal comfort and outdoor activities: A review of research in

850   the past decade," *Cities*, vol. 29, no. 2, pp. 118–125, 2012.

851   [35]   K. Rashidi, M. Stadelmann, and A. Patt, "Creditworthiness and climate: Identifying a hidden

852   financial co-benefit of municipal climate adaptation and mitigation policies," *Energy Res.*

853   *Soc. Sci.*, vol. 48, no. October 2018, pp. 131–138, 2019.

854   [36]   O. Potchter, P. Cohen, T.-P. Lin, and A. Matzarakis, "Outdoor human thermal perception in

855   various climates: A comprehensive review of approaches, methods and quantification," *Sci.*

856   *Total Environ.*, vol. 631–632, pp. 390–406, 2018.

857 [37] M. Kottek, J. Grieser, C. Beck, B. Rudolf, and F. Rubel, "World map of the Köppen-Geiger

858 climate classification updated," *Meteorol. Zeitschrift*, vol. 15, no. 3, pp. 259–263, 2006.

859 [38] I. Pigliautile and A. L. Pisello, "A new wearable monitoring system for investigating

860 pedestrians' environmental conditions: Development of the experimental tool and start-up

861 findings," *Sci. Total Environ.*, vol. 630, 2018.

862 [39] F. Salata, I. Golasi, R. de Lieto Vollaro, and A. de Lieto Vollaro, "Urban microclimate and

863 outdoor thermal comfort. A proper procedure to fit ENVI-met simulation outputs to

864 experimental data," *Sustain. Cities Soc.*, vol. 26, pp. 318–343, 2016.

865 [40] G. Battista, E. Carnielo, and R. De Lieto Vollaro, "Thermal impact of a redeveloped area on

866 localized urban microclimate: A case study in Rome," *Energy Build.*, vol. 133, pp. 446–454,

867 2016.

868 [41] M. Bruse and H. Fleer, "Simulating surface-plant-air interactions inside urban environments

869 with a three dimensional numerical model," *Environ. Model. Softw.*, vol. 13, no. 3–4, pp.

870 373–384, 1998.

871 [42] R. Taesler and C. Andersson, "A method for solar radiation computations using routine

872 meteorological observations," *Energy Build.*, vol. 7, no. 4, pp. 341–352, 1984.

873 [43] A. Zhang, R. Bokel, A. van den Dobbelsteen, Y. Sun, Q. Huang, and Q. Zhang, "An integrated

874 school and schoolyard design method for summer thermal comfort and energy efficiency in

875 Northern China," *Build. Environ.*, vol. 124, pp. 369–387, 2017.

876 [44] V. L. Castaldo, A. L. Pisello, I. Pigliautile, C. Piselli, and F. Cotana, "Microclimate and air

877 quality investigation in historic hilly urban areas: Experimental and numerical investigation

878 in central Italy," *Sustain. Cities Soc.*, vol. 33, 2017.

879 [45] D. B. Crawley, C. O. Pedersen, L. K. Lawrie, and F. C. Winkelmann, "Energy plus: Energy

880   simulation program," *ASHRAE J.*, vol. 42, pp. 49–56, 2000.

881 [46] UK Department for Communities and Local Government (DCLG), "UK's National Calculation

882   Method for Non Domestic Buildings," 2004. .

883 [47] "EN 15251:2007 - Indoor Environmental Input Parameters for Design and Assessment of

884   Energy Performance of Buildings Addressing Indoor Air Quality, Thermal Environment,

885   Lighting and Acoustics." 2007.

886 [48] C. A. Gueymard and D. R. Myers, "Validation and Ranking Methodologies for Solar Radiation

887   Models BT - Modeling Solar Radiation at the Earth's Surface: Recent Advances," V. Badescu,

888   Ed. Berlin, Heidelberg: Springer Berlin Heidelberg, 2008, pp. 479–510.

889 [49] J. E. Hay, "Calculation of monthly mean solar radiation for horizontal and inclined surfaces,"

890   *Sol. Energy*, vol. 23, no. 4, pp. 301–307, 1979.

891 [50] G. Emmi, R. Perego, S. Pera, M. De Carli, M. Cultrera, D. Mendrinos, S. Graci, A. Di Bella, R.

892   Pasquali, A. Zarrella, A. Galgaro, G. Mezzasalma, G. Dalla Santa, and A. Bernardi, "A

893   Database for Climatic Conditions around Europe for Promoting GSHP Solutions,"

894   *Geosciences*, vol. 8, no. 2, p. 71, 2018.

895 [51] IPCC, "Climate Change 2013," 2013.

896 [52] Intergovernmental Panel on Climate Change, Ed., "Summary for Policymakers," in *Climate

897   Change 2013 – The Physical Science Basis: Working Group I Contribution to the Fifth

898   Assessment Report of the Intergovernmental Panel on Climate Change*, Cambridge:

899   Cambridge University Press, 2014, pp. 1–30.

900 [53] A. Matzarakis, F. Rutz, and H. Mayer, "Modelling radiation fluxes in simple and complex

901   environments: Basics of the RayMan model," *Int. J. Biometeorol.*, vol. 54, no. 2, pp. 131–

902   139, 2010.

903   [54]   A. Matzarakis, F. Rutz, and H. Mayer, "Modelling the thermal bioclimate in urban areas with

904   the RayMan Model," *Energy*, vol. 6–8, Jan. 2006.

905   [55]   R. G. Steadman, "A Universal Scale of Apparent Temperature," *J. Appl. Meteorol. - J APPL*

906   *METEOROL*, vol. 23, no. 12, pp. 1674–1687, Dec. 1984.

907   [56]   Austrialian Government- Bureau of Meteorology, "Thermal Comfort observations," 2010. .

908   [57]   R. G. Steadman, "Norms of Apparent Temperature in Australia," *Aust. Meteorol. Mag.*, vol.

909   43, pp. 1–16, Jan. 1994.

910   [58]   H. PR, "The physiological equivalent temperature - A universal index for the

911   biometeorological assessment of the thermal environment," *Int. J. Biometeorol.*, vol. 43, no.

912   2, pp. 71–75, Nov. 1999.

913   [59]   S. Coccolo, J. Kämpf, J.-L. Scartezzini, and D. Pearlmutter, "Outdoor human comfort and

914   thermal stress: A comprehensive review on models and standards," *Urban Clim.*, vol. 18, pp.

915   33–57, 2016.

916   [60]   P. Cohen, O. Potchter, and A. Matzarakis, "Human thermal perception of Coastal

917   Mediterranean outdoor urban environments," *Appl. Geogr.*, vol. 37, no. 1, pp. 1–10, 2013.

918   [61]   A. Matzarakis, F. Rutz, and H. Mayer, "Modelling radiation fluxes in simple and complex

919   environments - Application of the RayMan model," *Int. J. Biometeorol.*, vol. 51, no. 4, pp.

920   323–334, 2007.

921   [62]   A. Pyrgou, V. L. Castaldo, A. L. Pisello, F. Cotana, and M. Santamouris, "Differentiating

922   responses of weather files and local climate change to explain variations in building

923   thermal-energy performance simulations," *Sol. Energy*, vol. 153, pp. 224–237, 2017.

924   [63]   A. Pyrgou, V. L. Castaldo, A. L. Pisello, F. Cotana, and M. Santamouris, "On the effect of

925   summer heatwaves and urban overheating on building thermal-energy performance in

926   central Italy," *Sustain. Cities Soc.*, vol. 28, pp. 187–200, 2017.

927   [64]   M. Belardi, *Il Palazzo dei consoli a Gubbio e il centro urbano trecentesco (in Italian)*. Perugia,

928   2001.

929